Int. J. Heat Mass Transfer. Vol 9, pp. 649–662. Pergamon Press 1966. Printed in Great Britain

HEAT TRANSFER BY NATURAL CONVECTION BETWEEN CONCENTRIC SPHERES

E. H. BISHOP†, L. R. MACK and J. A. SCANLAN
The University of Texas, Austin, Texas

(*Received* 27 *April* 1965 *and in revised form* 6 *September* 1965)

Abstract—An experimental investigation is described concerning natural convection of air enclosed between two isothermal concentric spheres of various diameter ratios ranging from 1·19 to 3·14. Results of a visual study, which indicated three distinct types of flow patterns, are summarized. Measured temperature profiles are analysed in detail with reference to five typical characteristics of the profile shapes. Except for the postulating of a bicellular flow to explain the profiles obtained for the smallest diameter ratio, all features of the profiles are explained in terms of the observed convective flow patterns. Two Nusselt–Grashof correlations are presented for the measured heat-transfer data for four different diameter ratios, the better correlation fitting the data within 15·5 per cent. The Grashof number based on gap thickness ranged from $2{\cdot}0 \times 10^4$ to $3{\cdot}6 \times 10^6$.

NOMENCLATURE

$a, b, c,$ constants in equation (5);
$A, B,$ constants in equation (9);
$c_p,$ specific heat at constant pressure;
$C_1, C_2,$ constants in equation (4);
$g,$ acceleration due to gravity;
$k,$ thermal conductivity;
$k_{\text{eff}},$ effective thermal conductivity;
$L,$ gap thickness, $r_o - r_i$;
N_{Gr} Grashof number, $g\beta L^3(\Delta T)/\nu^2$;
$N_{Nu},$ Nusselt number defined by equation (1);
$N^*_{Nu},$ Nusselt number ($= k_{\text{eff}}/k$) defined by equation (7);
$N_{Pr},$ Prandtl number, $c_p\mu/k$;
$q_c,$ natural convection heat-transfer rate, energy/time;
$q_L,$ rate of heat loss from inner sphere due to conduction along the stem and to radiation, energy/time;
$r,$ radial coordinate;
$r_{av},$ average radius, $(r_o + r_i)/2$;
$r_i,$ radius of inner sphere;
$r_o,$ radius of outer sphere;
$T,$ temperature;
$T_i,$ temperature of inner sphere;
$T_m,$ mean temperature defined by equation (2);
$T_o,$ temperature of outer sphere;
$\Delta T,$ temperature difference, $T_i - T_o$;
$\beta,$ coefficient of thermal expansion;
$\mu,$ dynamic viscosity;
$\nu,$ kinematic viscosity;
$\phi,$ angular coordinate, measured from upward vertical.

1. INTRODUCTION

HEAT transfer by natural convection from a body to its finite enclosure is an area in which relatively few studies have been published. Accurate prediction of such heat-transfer rates, which can now be only roughly approximated, is required in many engineering design problems. Certain boundary-layer approximations and simplifying assumptions regarding pressure gradients are generally made in analyses of simple bodies in an infinite atmosphere; however, these are not valid for enclosures, so that the analytical treatment of natural convection within even the simplest of enclosures is very difficult. Among the more important analyses of natural convection within enclosures are those by Batchelor [1] and Poots [2] of a rectangular cavity with heat

†Now at Mississippi State University, State College, Mississippi.

flow through the vertical faces and by Weinbaum [3] of a horizontal circular cylindrical cavity with a sinusoidally distributed wall temperature. The studies by Batchelor and Poots did not consider a body within the enclosure, while Weinbaum, although he did consider the case of a rotating inner cylinder whose thermal conductivity is the same as that of the surrounding fluid, had no net heat transfer from his enclosed body. Numerical integration of the governing equations for steady laminar convection between horizontal concentric circular cylinders was presented by Crawford and Lemlich [4], together with an analytical result for the case of creeping flow, and by Abbott [5]; while Wilkes and Churchill [6] gave finite-difference computations on the transient development of convection within a rectangular enclosure.

Many experimental investigations of convective heat transfer between parallel isothermal boundaries, placed either horizontally or vertically, are summarized by Jakob [7]; significant extensions have been made by Eckert and Carlson [8], by Dropkin and Somerscales [9], and by Emery and Chu [10]. The natural convection heat transfer within horizontal cylindrical annuli, a geometrical configuration closely related to that of the present study, has been investigated experimentally by Beckmann [11], by Kraussold [12], and more recently by Liu, Mueller and Landis [13].

The present paper presents the results of an experimental investigation of natural convection of air which is enclosed between two concentric spheres, each of which is maintained at a constant and uniform temperature. The apparatus was operated at several values of the ratio of the sphere diameters and for various differences in temperature between the heated inner sphere and the cooled outer sphere. Three distinct types of flow patterns, photographed and initially described by Bishop, Kolflat, Mack and Scanlan [14], are briefly discussed. For convenience of discussion the measured profiles of T vs. r are divided into five portions, each of which is characterized by a typical feature of the profile shape. Analysis is made of the variation, with respect both to ϕ and to L/r_i, of the radial extent of each portion and of the magnitude of its characterizing feature. All features of the profiles are explained in terms of the observed convective flow patterns, except that in order to explain the temperature profiles for the smallest gap a bicellular flow pattern is postulated. One Nusselt–Grashof correlation obtained for the heat-transfer measurements involves L/r_i explicitly and fits the data within 25·5 per cent. By use of the concept of k_{eff}/k, a simpler Nusselt–Grashof correlation is developed which involves L/r_i only implicitly and fits the data within 15·5 per cent.

2. HEAT-TRANSFER APPARATUS

The heat-transfer apparatus, shown schematically in Fig. 1, consisted of two concentric spheres enclosed in a water jacket. A single outer sphere of 10 inch diameter was used in conjunction with inner spheres of 4, 5, 6, and 8 inch diameters. These provided values of 1·50, 1·00, 0·67, and 0·25 for the gap–radius ratio L/r_i. All spheres were of $\frac{1}{16}$-inch-thick copper. The chromium plated inner spheres were mounted on a 1-inch-diameter Teflon stem. A uniform surface temperature of the inner sphere was achieved by condensing saturated Freon-11 vapor on the inner surface of the sphere; a check prior to final design indicated that the condensing vapor could maintain isothermality within $\frac{1}{4}$–$\frac{1}{2}$ degF. The saturation conditions were varied by means of a bare nichrome wire heater, wound in a flat spiral, which was located within the inner sphere below the Freon liquid level. The inner-sphere surface temperature was measured by a thermocouple located at the equator of the sphere. A small stainless-steel tube extended through the heater support for pressure measurements within the inner sphere.

The outer sphere consisted of two hemispheres joined by an external flange which was sealed with an O-ring to facilitate disassembly for changing the inner sphere. The inner sur-

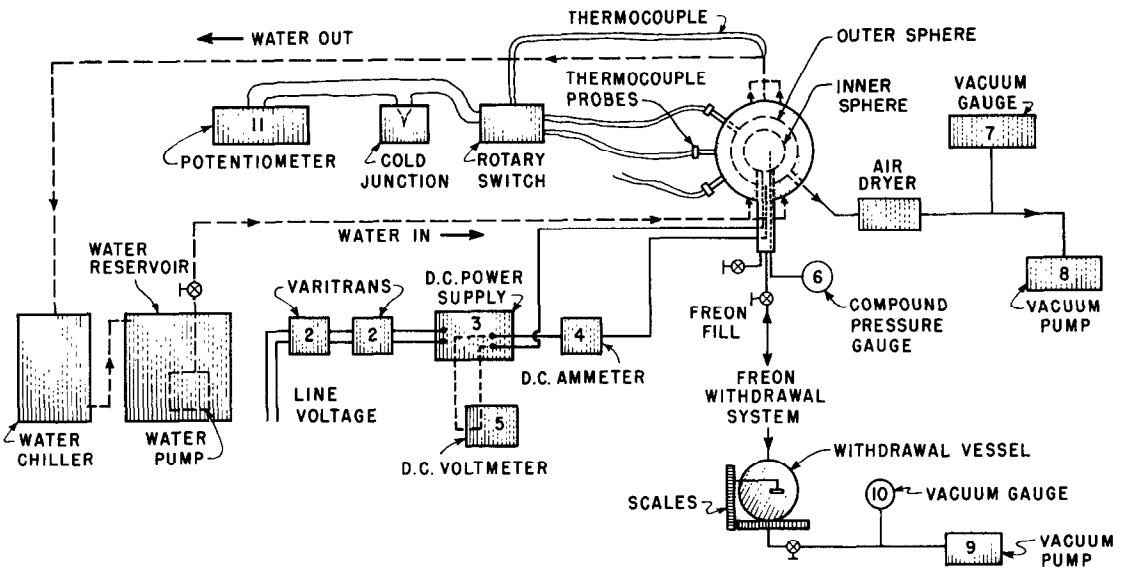

FIG. 1. Schematic diagram of heat-transfer apparatus.

faces of these hemispheres were gold plated to minimize radiation heat transfer. Thermocouple probe guides extended from the outer sphere through the water jacket. The outer sphere was supported within the water jacket by a 1 inch insulated brass tube. The Teflon and brass supporting tubes served as a Freon reservoir, and the brass tube also provided means of connecting electrical leads to the nichrome heater, leads to the inner-sphere surface thermocouple, and the pressure probe to instrumentation.

The water jacket was made of two, 14 in. dia., cadmium plated, steel hemispheres joined by an external gasketed flange to permit disassembly and was insulated to insure minimum heat loss to the surroundings. The assembled apparatus was mounted in gimbals to allow inversion during purging and Freon charging. The water, which maintained the outer sphere at a uniform temperature, was introduced at the base and withdrawn at the top through a manifold system. The outer-sphere surface temperature was taken to be the average of the inlet and outlet water temperatures, which were measured by thermocouples. The average change in temperature of the jacket water was $\frac{1}{2}$ degF.

The thermocouple probes used to obtain the temperature profiles were constructed by inserting 30-gauge copper and constantan wires through 15-gauge stainless-steel support tubes and fusing the wires by electrical means to form small junctions. The junctions were placed approximately $\frac{3}{32}$ inch beyond the end to the support tubes, and the wires were then sealed to the tubes at both ends with epoxy cement. Each support tube was attached to a micrometer probing mechanism which advanced the thermocouple probe 0·025 inch per turn. On the basis of visual observations, which indicated no cross flow, made in a similar transparent flow apparatus described by Bishop, Kolflat, Mack and Scanlan [14], the flow was treated as axisymmetric. Accordingly, five thermocouple probes were located in a common vertical plane through the center of the spheres. These were spaced at 40° intervals beginning with a probe on the upward vertical axis.

3. PROCEDURE

Since only heat transfer by natural convection was being sought, it was necessary to determine the radiation transfer between the spheres and the conduction loss through the supporting

stems. This calibration was done by evacuating the gap between the spheres to a pressure of about 40 μm Hg. At this pressure the Grashof number N_{Gr} and the thermal conductivity k [15] of the air were only about 5×10^{-9} and 5×10^{-2}, respectively, of their values at atmospheric pressure. By maintenance of a constant outer-sphere temperature (45°F) for the calibration, the sum q_L of the radiation and stem-conduction losses becomes a function of the temperature of only the inner sphere and is essentially equal to the total heat input to the Freon. The power input to the heater was set to a sufficient number of values to permit plotting a calibration curve for each L/r_i over the anticipated range of inner-sphere temperatures. From 20 to 40 hr were allowed for each calibration point to assure steady-state conditions. Since the plots of q_L vs. T_i are linear (see Fig. 2), the

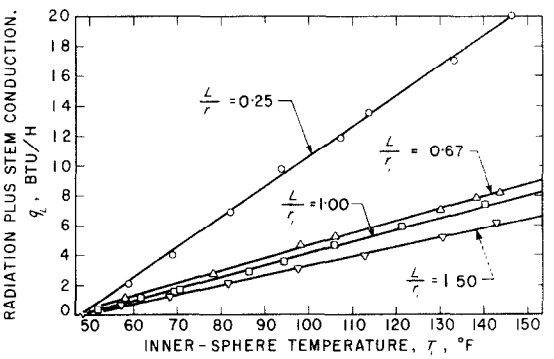

FIG. 2. Calibration curves giving heat transfer by radiation and stem conduction for each L/r_i.

correction for stem conduction is apparently much greater than that for radiation transfer. The general ordering of the curves is consistent with this observation. However, the spacing of the curves with respect to changes in L/r_i is slightly inconsistent, possibly because of conduction through the air remaining in the gap.

About 70 heat-transfer runs were conducted with dried air at atmospheric pressure in the gap. At each of the four gap-radius ratios, 14–20 different values of ΔT were established by controlling the electrical power input to the heater. Approximately 10–15 hr were allowed for establishment of a steady state before each run. The outer sphere was maintained at the same temperature as that used for the calibration so that the curves of Fig. 2 could be used to predict q_L at a variety of inner-sphere temperatures. For the heat-transfer runs q_L varied from 12·5 to 23·5 per cent of the total power input to the heater, the proportion decreasing as ΔT increased. At selected temperature differences (low, intermediate, and high) for each gap–radius ratio, temperature traverses were made utilizing the thermocouple probes.

4. FLOW PATTERNS

Since fluid flow is a part of all convection problems, it was realized that careful observations of the flow were necessary in order to gain a better understanding of the measured heat-transfer rates and temperature distributions. Hence a transparent apparatus was constructed similar to the metallic apparatus described in Section 2. The values of L/r_i of the transparent apparatus did not coincide exactly with those of the metallic apparatus, but the same range of values was used. Visual observations of the flow, made visible by smoke particles, were made, supplemented by photographs obtained by a technique described by Bishop, Kolflat, Mack and Scanlan [16]. Representative pictures of the flows corresponding to various operating conditions, together with a detailed discussion of the flow patterns, have been given by Bishop, Kolflat, Mack and Scanlan [14]. A summary of the results of the flow visualization study follows.

Three distinct types of flow were observed in the ranges of L/r_i and ΔT investigated. The most common pattern, the "crescent-eddy" type, is shown in Fig. 3. This pattern occurred for gap–radius ratios of 0·37 and 0·72 at all temperature differences studied, while for ratios 0·19, 1·53 and 2·14 it occurred only at small temperature differences. Very close to each sphere was a thin layer of rapidly moving fluid resembling a boundary layer, while the central crescent eddy consisted of slowly moving fluid.

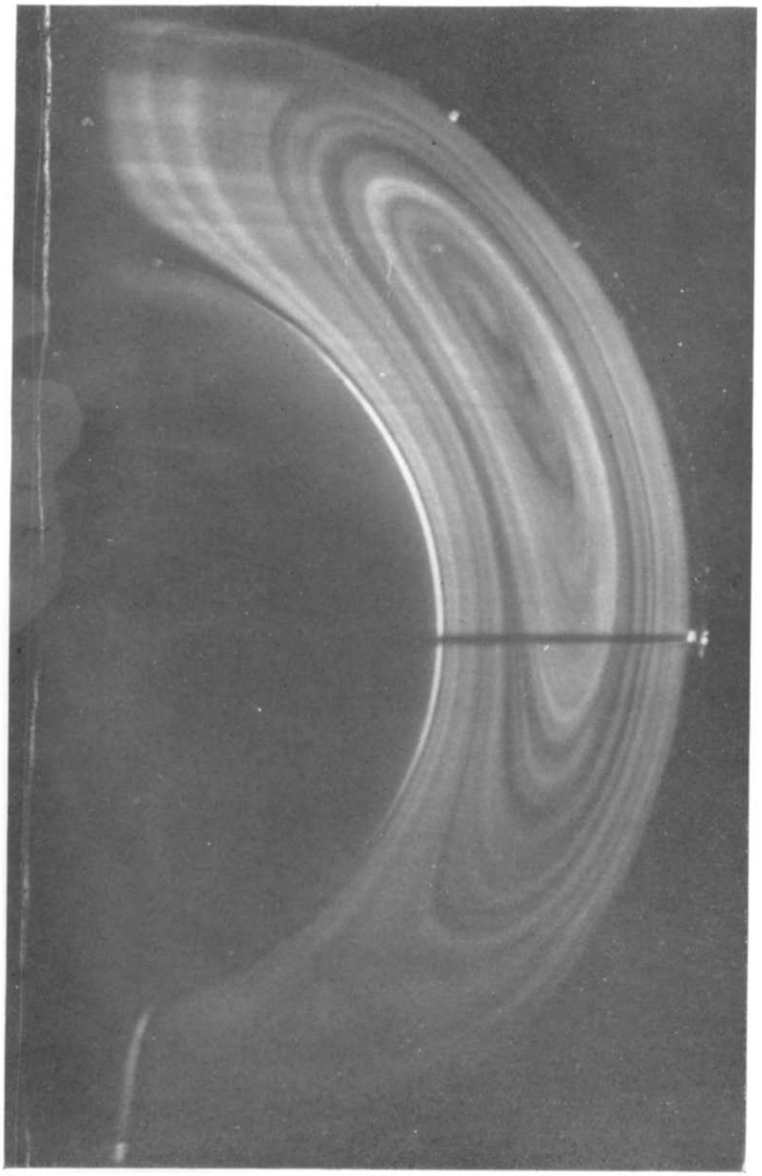

FIG. 3. Crescent-eddy flow pattern for $L/r_i = 0{\cdot}72$, $\Delta T = 15$ degF.

[*facing page 652*

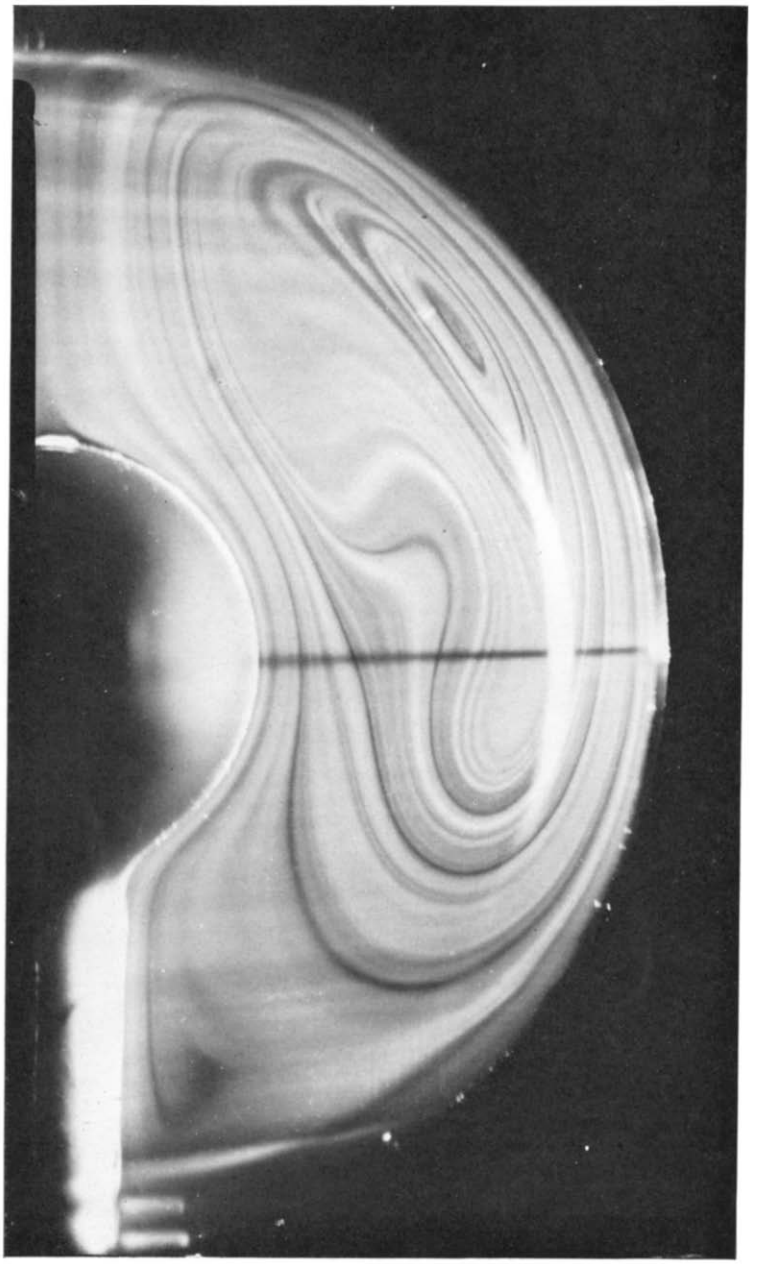

FIG. 5. Kidney-shaped-eddy flow pattern for $L/r_i = 2{\cdot}14$, $\Delta T = 30$ degF.

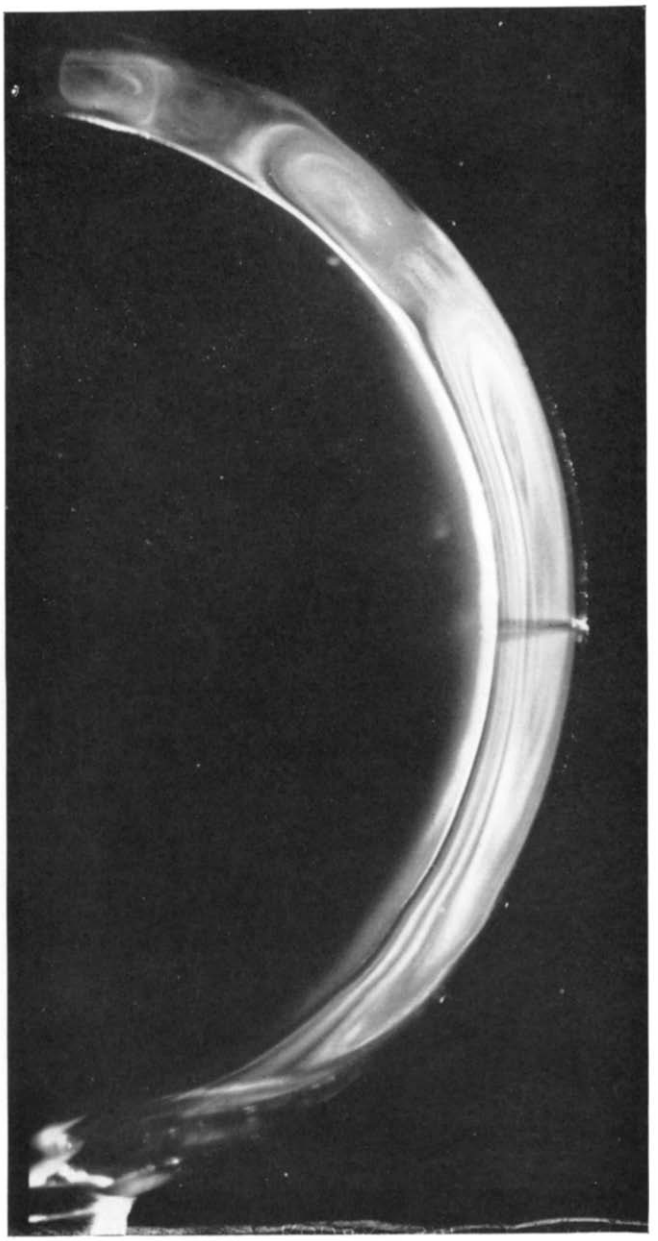

FIG. 6. One phase of the falling-vortices flow pattern for $L/r_i = 0{\cdot}19$, $\Delta T = 15$ degF.

The upward velocities adjacent to the inner sphere were considerably greater than the downward velocities along the outer sphere. In the lower region essentially the entire gap between the spheres was filled with relatively stagnant fluid. At the top of the inner sphere the high-speed flow separated from the inner sphere, as is visible in Fig. 3, leaving a corner eddy adjacent to the intersection of the surface of the inner sphere with the vertical axis of symmetry. The flow in the corner-eddy region is indicated schematically in Fig. 4. This portion of the flow

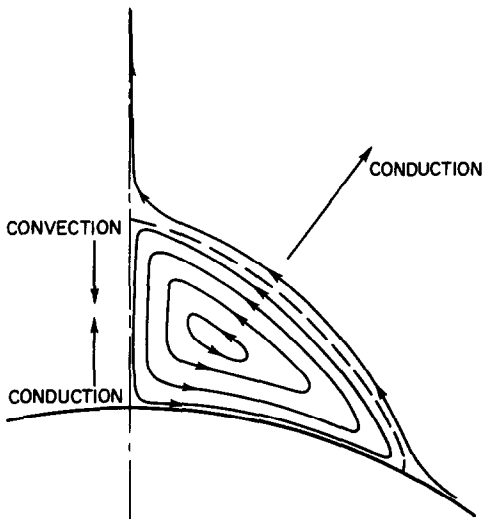

FIG. 4. Schematic of corner eddy.

will be discussed further in Section 5 in conjunction with the temperature distribution.

The second flow pattern, the "kidney-shaped-eddy" type, is a modification of the crescent-eddy type of flow. It occurred for gap–radius ratios of 1·53 and 2·14 at moderate to large temperature differences. In this type, the central low-speed region is no longer crescent shaped but has become distorted into a kidney shape (Fig. 5), the distortion from the crescent shape becoming more pronounced with increasing temperature difference. It should be emphasized that this flow pattern, like the crescent-eddy type, is completely steady in time. Since the kidney-eddy type differs qualitatively from the crescent-eddy type only in the shape of the flow lines in the low-speed central-eddy region, it is reasonable to expect the heat-transfer characteristics of the two types to be similar.

The third flow pattern observed, the "falling-vortices" type, occurred at moderate to high temperature differences for the lowest gap–radius ratio studied (0·19). This flow is unsteady, characterized by the formation and shedding of small vortex cells. These vortices appeared to form in counter-rotating pairs in the upper region adjacent to the vertical axis of symmetry. Upon the formation of a second pair of counter-rotating cells, all four cells began, as shown in Fig. 6, to merge into an elongated shape which then appeared to drain into the outer-sphere boundary flow while at the same time the central eddy rose. This action resulted in a momentary reversion to the single-crescent-eddy type of flow pattern, which immediately began to break into vortex cells as before. The formation and shedding of the vortex cells appeared to be periodic with a period of approximately 9–12 s.

The crescent-eddy and kidney-eddy types of flow are steady, whereas the falling-vortices type is unsteady. In all three types the central eddy involves a cellular type of motion. The falling-vortices type is multicellular because of the presence of the smaller vortex cells in addition to the central eddy. On the other hand, the crescent-eddy and kidney-eddy types will be called monocellular inasmuch as the corner eddy is not of trans-gap extent.

5. TEMPERATURE DISTRIBUTION

Profiles of temperature T versus radial position r were obtained at selected temperature differences and angular positions for each gap–radius ratio. The form of the dimensionless temperature profile for a given angular position ϕ, measured from the upward vertical, appears (as is shown in Fig. 7 for $L/r_i = 1{\cdot}00$) to be essentially independent of the temperature difference ΔT for those combinations of ΔT and L/r_i which

give flow patterns of types other than the falling-vortices type. Thus dimensionless temperature profiles are presented for only one ΔT at each L/r_i (Figs. 8–11). On each of Figs. 7 through 11 the temperature distribution for simple conduction is shown for comparison. (Since all temperature profiles presented here are dimensionless, the adjective "dimensionless" will not henceforth be used.)

General observations—that is, those that are valid for *most* values of L/r_i—will be discussed first. Next comes comment on phenomena associated with particular values of L/r_i, pointing out exceptions to the general observations. Trends with respect to variations of L/r_i will then be noted.

Each temperature profile exhibits an approximately similar shape which may be characterized by five individual regions, each of which may vary, both in radial extent and in the magnitude of its characterizing feature, with ϕ and L/r_i. The region immediately adjacent to the inner sphere is an extremely thin one in which a precipitous drop in temperature occurs. The

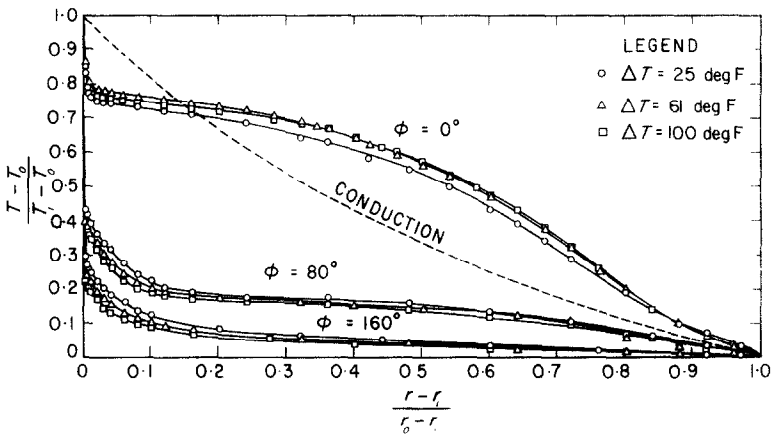

FIG 7. Variation of dimensionless temperature profiles with ΔT at selected angular positions for $L/r_i = 1{\cdot}00$.

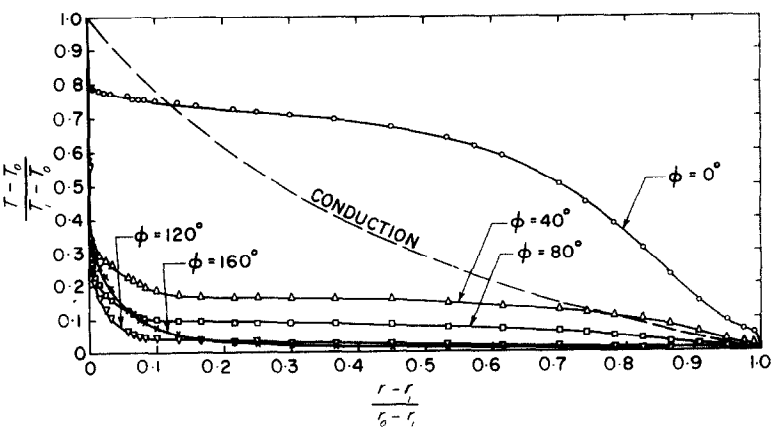

FIG. 8. Dimensionless temperature profiles for $L/r_i = 1{\cdot}50$, $\Delta T = 100$ degF.

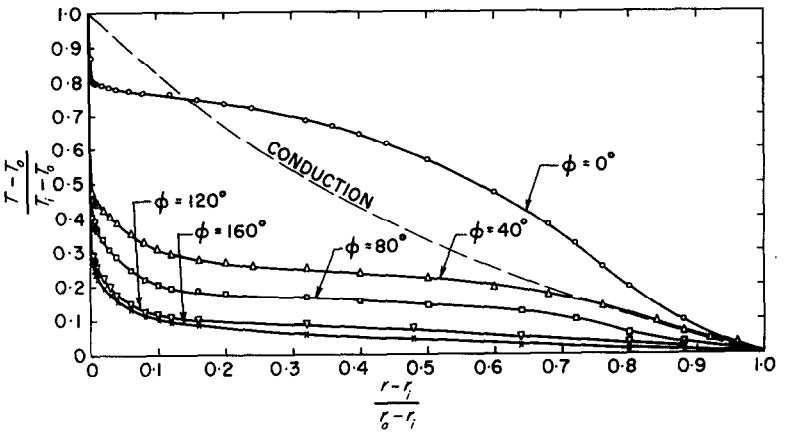

FIG. 9. Dimensionless temperature profiles for $L/r_i = 1{\cdot}00$, $\Delta T = 61$ degF.

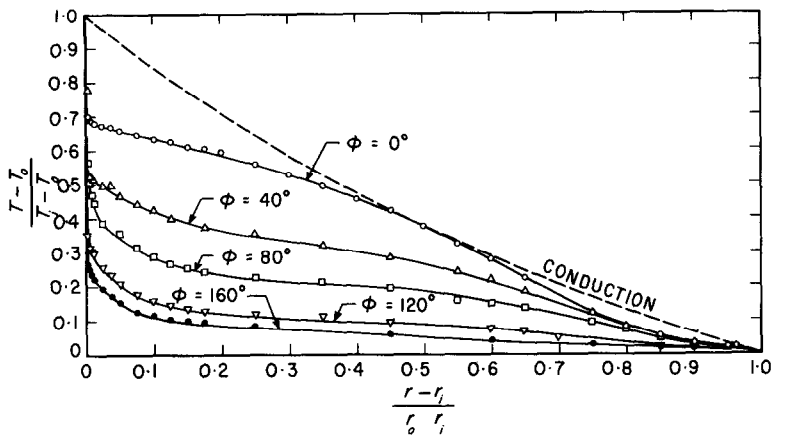

FIG. 10. Dimensionless temperature profiles for $L/r_i = 0{\cdot}67$, $\Delta T = 57$ degF.

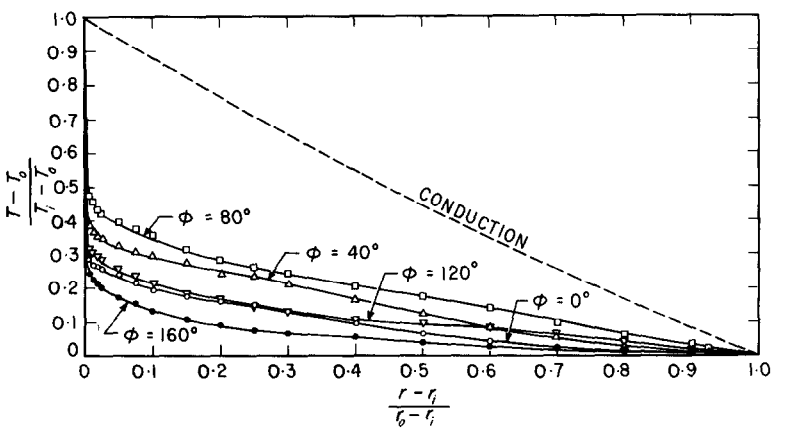

FIG. 11. Dimensionless temperature profiles for $L/r_i = 0{\cdot}25$, $\Delta T = 56$ degF.

second region is characterized by a large curvature of the profile. Occupying most of the gap is the third region, in which the temperature gradient is small and relatively uniform. Near the outer sphere, another curvature region is encountered which is, however, generally of much smaller radial extent than the inner-sphere curvature region. Although it is not evident in Figs. 7–11, the existence, immediately adjacent to the outer sphere, of the fifth region, in which the temperature drop is precipitous but extremely small in magnitude, is indicated (but not conclusively) by the original data. These characteristics of the temperature profiles correlate quite well with what might reasonably be expected based on the flow patterns.

The precipitous-drop regions, except at $\phi = 0°$, are due to the high rate with which heat is convected in the tangential direction, from the inner sphere and to the outer sphere, by the high-speed boundary layers immediately adjacent to the spheres. The magnitude of the precipitous drop at the inner sphere is always quite large, ranging from about 0·45 to about 0·75, while the drop at the outer sphere is always very small. One reason for the difference in magnitude of these two temperature drops is that the boundary-layer velocity adjacent to the inner sphere is much greater than that adjacent to the outer sphere.

The small-temperature-gradient region, except at $\phi = 0°$, is associated with the low-speed central-eddy region of flow (which does not extend to the upward vertical) regardless of whether the central eddy is of crescent or kidney-shaped type. Note that the magnitude of the temperature in this region increases with decreasing ϕ. This is because the fluid on the inner-sphere side of the central eddy is continuously exposed to radial conduction of heat from the inner sphere as it rises; similar reasoning, appropriately modified, applies to the outer-sphere side.

Note that the magnitude of the inner-sphere precipitous drop decreases with decreasing value of ϕ. Since the temperature on the inner-sphere side of the small-gradient region increases with decreasing ϕ, and since T_i is independent of ϕ, the total temperature drop across the inner-sphere precipitous-drop and curvature regions must decrease with decreasing ϕ. Because the ratio of the individual temperature drops across these two regions does not change radically with ϕ, the fact that the total drop across these two regions decreases with decreasing ϕ requires that the magnitude of the inner-sphere precipitous drop decrease with decreasing ϕ.

The inner-sphere and outer-sphere curvature regions, except at $\phi = 0°$, represent the regions of transition of the velocity from the high-speed boundary layer flows to the low-speed flow within the central-eddy region.

The shape of the profiles at $\phi = 0°$ is due to other causes. The fluid at the upstream edge of the corner eddy has received maximum heating from the inner sphere. As this fluid then flows adjacent to the streamline separating the main flow from the corner eddy, it loses heat toward the outer sphere by conduction (Fig. 4), becoming partially cooled by the time it reaches the vicinity of the vertical axis of symmetry. The partially cooled fluid in the corner eddy then flows toward the heated inner sphere adjacent to the vertical axis. In this flow of partially cooled fluid toward the inner sphere, the upward heat transfer by conduction and the downward heat transport by convection are in opposite senses (Fig. 4). This accounts for the inner-sphere precipitous drop, for the very small radial extent of the inner-sphere curvature region (about one-sixth to one-fourth of its extent for general ϕ), and for the flatness of the temperature profiles just beyond the curvature region at $\phi = 0°$. The remaining portions of the profiles at $\phi = 0°$ are related to the fact that, in the zone adjacent to the vertical axis between the corner eddy and the outer sphere, there is a rapidly rising column of fluid within which the heat transfer by conduction and the heat transport by convection are both toward the outer sphere.

The discussion of those features of the temperature profiles which are typical for most

values of the gap–radius ratio now being finished, attention will next be given to phenomena associated with particular values of the gap–radius ratio. Exceptions to the general discussion of temperature profiles will also be noted.

For $L/r_i = 1{\cdot}50$ (Fig. 8), the temperature profile at $\phi = 160°$, in contrast to what was observed generally, has an inner-sphere precipitous drop of smaller magnitude than do those at $\phi = 120°$ and $\phi = 80°$ and also has an inner-sphere curvature region of both greater temperature drop and greater radial extent than do those for all other ϕs. For this value of L/r_i the temperature traverse at 160° passes through the lower, relatively stagnant flow region, so that the boundary-layer flow along the inner sphere is weak. Heat transfer by radial conduction thus partially overrides that by convection; this explains the atypical character of this profile. On the basis of visual observations, it is believed that this effect would be even more pronounced for larger values of L/r_i. The visual study ($L/r_i = 1{\cdot}53$) indicated that the flow pattern for this gap–radius ratio of 1·50 was of the kidney-shaped-eddy type for the temperature differences for which temperature profiles were obtained.

For $L/r_i = 1{\cdot}00$, no exceptions to the general observations were noted. For the values of ΔT for which temperature profiles were obtained, the kidney-eddy type of flow was observed visually for $L/r_i = 1{\cdot}53$, while the crescent-eddy type of flow was observed for $L/r_i = 0{\cdot}72$ (Fig. 3). The flow for $L/r_i = 1{\cdot}00$ could thus be either of these types.

Likewise for $L/r_i = 0{\cdot}67$, no exceptions to the general features of the temperature profiles were noted. However, small (about $\frac{1}{2}$–1 degF) temperature fluctuations occurred at $\phi = 0°$, 40° and 80°, most likely caused by flow irregularities which were too small to be discernible by visual observation. The flow pattern for this gap–radius ratio is the crescent-eddy type.

For $L/r_i = 0{\cdot}25$, fluctuations in temperature occurred for all traverses. For low and intermediate values of ΔT (18 and 56 degF) these fluctuations were small (about 2–3 degF), primarily affecting the profiles at $\phi = 0°$ and 40°, while for high ΔT (100 degF) they were so large for all values of ϕ that a meaningful temperature profile for this ΔT could not be obtained. It should be emphasized that the profiles obtained for temperature differences of 18 and 56 degF are essentially identical.

The temperature profiles obtained for $L/r_i = 0{\cdot}25$ (Fig. 11) do not follow the general pattern. For one thing, neither an outer-sphere curvature region nor an outer-sphere precipitous-drop region was indicated. Furthermore, the inner-sphere curvature region for each ϕ has a radial extent only about half as great as it does in general, so that the small-gradient region came much nearer to occupying the entire gap. Instead of having by far the smallest inner-sphere precipitous drop, as it does in general, the profile for $\phi = 0°$ in this case has next to the largest temperature drop. Within experimental accuracy, the temperature at every radial position within the gap was greatest for $\phi = 80°$, next greatest for $\phi = 40°$, followed by 120°, 0°, and 160° in that order. This ordering of the magnitudes of T for $\phi = 0°$ and 40°, relative both to each other and to those for the other angular positions, is almost totally different from that of any other gap–radius ratio; however, the ordering of the magnitudes of T for $\phi = 80°$, 120°, and 160° relative to each other does follow the general rule.

The behavior of the temperature profiles for $L/r_i = 0{\cdot}25$ could not be explained in terms of the flow patterns observed in the visual work. Visual observations of the flow for $L/r_i = 0{\cdot}37$ showed the crescent-eddy type of flow for all temperature differences studied, while for $L/r_i = 0{\cdot}19$ the falling-vortices type was observed for temperature differences of 15 degF or more. Since a gap–radius ratio of 0·25 is intermediate between these two, its flow pattern might reasonably be expected to be one of these types. However, the fact that the previously noted temperature fluctuations affected only the traverses at $\phi = 0°$ and 40° rules out the falling-vortices type of flow, and the crescent-eddy flow pattern

could not possibly give the temperature profiles measured for $L/r_i = 0{\cdot}25$.

We therefore postulate for $L/r_i = 0{\cdot}25$ a bicellular flow pattern in which the division between the main central cellular flow in the lower (and major) portion of the gap and a secondary cellular flow in the upper (and minor) portion of the gap occurs somewhere between $\phi = 80$ and $\phi = 40°$, as shown in Fig. 12. This bicellular flow

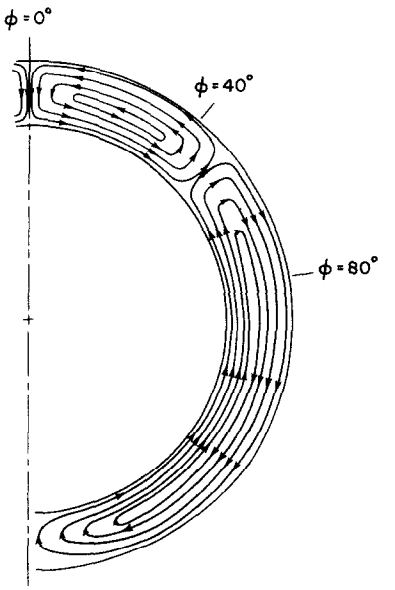

FIG. 12. Postulated bicellular flow pattern for $L/r_i = 0{\cdot}25$.

—a particular type of multicellular flow—would yield temperature profiles consistent with those shown in Fig. 11.

Trends with respect to variations of L/r_i will now be noted. Since the temperature distributions for the gap–radius ratio (0·25) for which the flow pattern was postulated to be bicellular are quite different from those for gap–radius ratios corresponding to monocellular flow, the following discussion of trends is restricted, except where otherwise noted, to those L/r_i for which the flow is monocellular.

Comparison of the temperature distributions for the different gap–radius ratios shows that for all ϕ except $\phi = 0$ the magnitude of the inner-sphere precipitous drop tends to decrease as L/r_i decreases, this decrease in magnitude of the drop being greater for the smaller values of ϕ. Conversely, again for all ϕ except $\phi = 0$, the absolute magnitude of the slope in the small-temperature-gradient region increases with decreasing L/r_i, this increase being less noticeable between $L/r_i = 1{\cdot}5$ and $L/r_i = 1{\cdot}0$. This latter trend also extends to $L/r_i = 0{\cdot}25$ for which the flow is multicellular. Both of these trends are due to high velocities extending relatively farther into the gap and to the consequent reduction in relative size of the low-speed central-eddy region as the gap–radius ratio is reduced; these changes in the flow were observed visually.

In contrast to its trend for other values of ϕ, the magnitude of the inner-sphere precipitous drop at $\phi = 0°$ increases with decreasing gap radius ratio. An increase in relative size of the corner eddy as L/r_i is reduced would cause the fluid in the corner eddy adjacent to the separation streamline to be cooled for a relatively longer time, thus giving an increase in the magnitude of the precipitous drop at this angular position with decreasing L/r_i.

6. HEAT-TRANSFER RESULTS

The heat-transfer results obtained experimentally are analysed in terms of the Prandtl number N_{Pr}, the Grashof number N_{Gr}, and the gap–radius ratio L/r_i. Since air was the only fluid used, and since its Prandtl number does not vary significantly within the range of temperatures involved in this investigation ($\sim 45°$ F to $\sim 150°$ F), N_{Pr} is considered to have been constant.

The convective heat transfer rate q_c can be expressed in terms of a Nusselt number N_{Nu} defined as

$$N_{Nu} = \frac{q_c L}{4\pi k(\Delta T) r_i^2}. \qquad (1)$$

In the determination of N_{Nu} from equation (1), q_c is given by the difference between the total

power input to the heater and the sum q_L of the radiation and stem-conduction losses (Fig. 2), and k was evaluated at a mean temperature T_m arbitrarily defined as

$$T_m = [(r_{av}^3 - r_i^3)T_i + (r_o^3 - r_{av}^3)T_o]/(r_o^3 - r_i^3) \quad (2)$$

So defined, T_m is a volume-weighted mean temperature in which each differential volume element within the gap is arbitrarily assigned the temperature of the nearer surface.

The functional relationship

$$N_{Nu} = f(N_{Gr}, L/r_i) \quad (3)$$

was sought. In analysing the experimental data, it was observed that plots of N_{Nu} vs. N_{Gr} using log–log coordinates gave a straight line for each L/r_i. Thus, the form of the correlating equations was assumed to be

$$N_{Nu} = C_1(N_{Gr})^{C_2} \quad (4)$$

where, for a particular value of L/r_i, C_1 and C_2 were constants to be determined. By means of a least-squares technique, correlating equations for each L/r_i were obtained that represented the experimental data with an acceptable degree of accuracy. It was observed that the exponent C_2 of the Grashof number varied between 0·217 and 0·348 for $0{\cdot}25 \leqslant L/r_i \leqslant 1{\cdot}50$ which indicated that the parameter L/r_i had a substantial influence on the heat-transfer rate.

An equation of the form

$$N_{Nu} = a(N_{Gr})^b\,(L/r_i)^c \quad (5)$$

was then assumed for overall correlation of the experimental results. By means of a least-squares technique, the constants a, b and c were determined, and the following correlating equation resulted:

$$N_{Nu} = 0{\cdot}332\,(N_{Gr})^{0{\cdot}270}\,(L/r_i)^{0{\cdot}517} \quad (6)$$

Applied to all of the data, equation (6) gave deviations ranging from −25·5 per cent to +14·6 per cent, where deviation is defined by

$$\text{Deviation} = [(N_{Nu})_{\text{equation}} - (N_{Nu})_{\text{data}}]/(N_{Nu})_{\text{data}}.$$

In analysing the deviations, it was found that the maximum occurred for $L/r_i = 0{\cdot}25$, for which the flow was postulated to be bicellular. Applied to only the data for those gap–radius ratios for which the flow was monocellular, equation (6) gave deviations ranging from −12·7 per cent to +14·6 per cent. The maximum deviations in this instance occurred for the runs made at the lowest ΔTs for each L/r_i, for which small experimental errors are magnified in the final determination both of N_{Nu} and of N_{Gr}.

Results of experiments concerning natural convection heat transfer within other shapes of enclosures suggest that a suitably selected form of correlation for concentric spheres may be relatively insensitive to the flow configuration. Thus, it should be possible to obtain an overall correlation which would give maximum deviations smaller than those given by equation (6).

To correlate the natural convection heat transfer between horizontal isothermal concentric cylinders, Beckmann [11], Kraussold [12], and Liu, Mueller and Landis [13] defined an "effective" thermal conductivity, which modified the simple conduction solution to account for convection. Applying their concept to the case of isothermal concentric spheres, we define a different Nusselt number N_{Nu}^* as

$$N_{Nu}^* = \frac{q_c L}{4\pi k(\Delta T) r_i r_o} \quad (7)$$

where $N_{Nu}^* = k_{\text{eff}}/k = N_{Nu}/[1 + (L/r_i)]$.

In functional form the heat-transfer results can be expressed as

$$N_{Nu}^* = f(N_{Gr}, L/r_i). \quad (8)$$

It was observed that plots of N_{Nu}^* versus N_{Gr} using log–log coordinates gave a straight line for each L/r_i and showed that N_{Nu}^* has only a weak dependence on L/r_i. Thus, the form of an overall correlating equation was assumed to be

$$N_{Nu}^* = A(N_{Gr})^B. \quad (9)$$

A least-squares technique was used to obtain the values of A and B in equation (9), the resulting

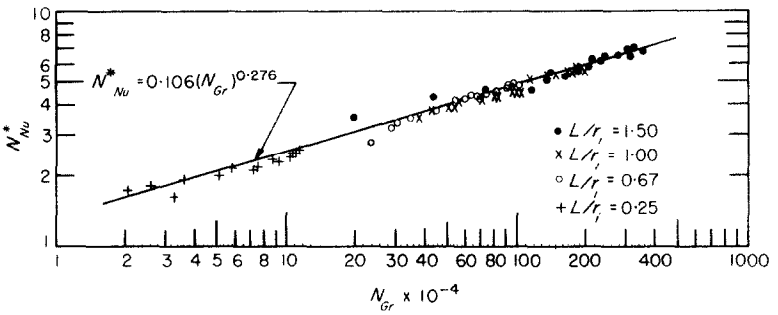

FIG. 13. Overall correlation of heat-transfer data.

correlating equation being

$$N^*_{Nu} = 0{\cdot}106(N_{Gr})^{0{\cdot}276}, \qquad (10)$$

which correlates all of the data with maximum deviations of −13·4 per cent and +15·5 per cent, as shown in Fig. 13.

The maximum deviations are for the runs at the small ΔTs; 94 per cent of the data are represented by equation (10) with maximum deviations of +5·9 per cent and −7·7 per cent. The five points with deviations greater than ±5·9 per cent all occurred among the lowest ΔTs at each L/r_i.

It is thus seen that equation (10) gives the better overall correlation, and hence it is the one which should be used to calculate the heat-transfer rate by natural convection between isothermal concentric spheres, with air in the enclosed space, for $0{\cdot}25 \leqslant L/r_i \leqslant 1{\cdot}50$ and $2{\cdot}0 \times 10^4 \leqslant N_{Gr} \leqslant 3{\cdot}6 \times 10^6$.

7. CONCLUSION

The measured temperature distributions were found to be relatively independent of the temperature difference both for those gap–radius ratios for which the flow pattern was monocellular, whether of the crescent-eddy type or the kidney-shaped-eddy type, and also for the gap–radius ratio for which the flow was multicellular. All temperature profiles were analysed in terms of five characteristic regions: an inner-sphere precipitous-drop region, an inner-sphere curvation region, a small-temperature-gradient region, and outer-sphere curvature and precipitous-drop regions. The manners in which these profiles varied both with angular position ϕ and with gap–radius ratio L/r_i were discussed, and exceptions to the general rules were noted. Except for the postulation of a bicellular flow to explain the temperature profiles obtained for the smallest gap–radius ratio (0·25), all features of the temperature profiles were explained in terms of the convective flow patterns previously reported [14].

Two Nusselt–Grashof relations, equations (6) and (10), were obtained which reasonably correlate the measured heat-transfer data. Equation (6), which incorporates L/r_i explicitly, involves three experimentally determined coefficients and fits the data within a maximum absolute deviation of 25·5 per cent. Equation (10), which incorporates L/r_i implicitly through the selection of N^*_{Nu} equivalent to k_{eff}/k, involves only two experimentally determined coefficients and fits within 15·5 per cent. Hence equation (10) is the recommended correlation.

To the authors' knowledge the work presented herein describes the only information available to date concerning natural convection heat transfer between isothermal concentric spheres. As such, attention has been directed only to the broad effects. Further study should be devoted to secondary effects such as the influence of the supporting stem and the role of the corner eddy in the transition from steady monocellular flow to steady and/or unsteady multicellular flow.

ACKNOWLEDGEMENTS

Figures 3, 5, and 6 and some phraseology in Section 4 are reproduced by permission of the copyright holders: Giedt and Levy, eds. *Proceedings of the* 1964 *Heat Transfer and Fluid Mechanics Institute*, Stanford University Press. This paper is based in part on a Ph.D. dissertation (E.H.B.) submitted to the Graduate School of The University of Texas.

REFERENCES

1. G. K. Batchelor, Heat transfer by free convection across a closed cavity between vertical boundaries at different temperatures, *Q. Appl. Math.* **12**, 209–233 (1954).
2. G. Poots, Heat transfer by laminar free convection in enclosed plane gas layers, *Q. Jl Mech. Appl. Math.* **11**, 257–273 (1958).
3. S. Weinbaum, Natural convection in a horizontal circular cylinder, *J. Fluid Mech.* **18**, 409–437 (1964).
4. L. Crawford and R. Lemlich, Natural convection in horizontal concentric cylindrical annuli, *I/EC Fundamentals* **1**, 260–264 (1962).
5. M. R. Abbott, A numerical method for solving the equations of natural convection in a narrow concentric cylindrical annulus with a horizontal axis, *Q. Jl Mech. Appl. Math.* **17**, 471–481 (1964).
6. J. O. Wilkes and S. W. Churchill, The finite difference computation of natural convection in a rectangular enclosure, *A.I.Ch.E. Jl* **12**, 161–166 (1966).
7. M. Jakob, *Heat Transfer*, Vol. 1. John Wiley, New York (1949).
8. E. R. G. Eckert and W. O. Carlson, Natural convection in an air layer enclosed between two vertical plates with different temperatures, *Int. J. Heat Mass Transfer* **2**, 106–120 (1961).
9. D. Dropkin and E. Somerscales, Heat transfer by natural convection in liquids confined by two parallel plates which are inclined at various angles with respect to the horizontal, *J. Heat Transfer* **87**, 77–84 (1965).
10. A. Emery and N. C. Chu, Heat transfer across vertical layers, *J. Heat Transfer* **87**, 110–116 (1965).
11. W. Beckmann, Die Warmeübertragung in zylindrischen Gasschichten bei naturlicher Konvektion, *Forsch. Geb. IngWes.* **2**, 165–178, 213–217, 407 (1931).
12. H. Kraussold, Warmeabgabe von zylindrischen Flussigkeitschichten bei naturlicher Konvektion, *Forsch. Geb. IngWes.* **5**, 186–191 (1934).
13. C.-Y. Liu, W. K. Mueller, and F. Landis, Natural convection heat transfer in long horizontal cylindrical annuli, *International Developments in Heat Transfer*, Part V, pp. 976–984. Amer. Soc. Mech. Engrs., New York (1961).
14. E. H. Bishop, R. S. Kolflat, L. R. Mack, and J. A. Scanlan, Convective heat transfer between concentric spheres, *Proc.* 1964 *Heat Transfer Fluid Mech. Inst.*, pp. 69–80. Stanford University Press (1964).
15. C. A. Whitehurst and W. H. Chapman, Research investigates thermal conductivity of natural air at very low pressures, *Heat. Pip. Air Condit.* **35**, 129–134 (1963).
16. E. H. Bishop, R. S. Kolflat, L. R. Mack and J. A. Scanlan, Photographic studies of convection patterns between concentric spheres, *Soc. Photo-Opt. Instrumn Engrs Jl* **3**, 47–49 (1964–1965).

Résumé—Les auteurs décrivent une étude expérimentale concernant la convection naturelle de l'air emprisonné entre deux sphères concentriques isothermes dont le rapport des diamètres varie de 1,19 à 3,14. Les résultats d'une visualisation qui a mis en évidence trois types différents de configuration d'écoulements, sont résumés. Les profils de température mesurés sont analysés en détail en relation avec cinq caractéristiques types de la forme des profils. En dehors de l'hypothèse d'un écoulement à deux cellules nécessaire pour expliquer les profils obtenus avec le rapport des diamètres le plus faible, toutes les caractéristiques des profils sont explicables à l'aide ces configurations observées de l'écoulement de convection. Deux corrélations du nombre de Nusselt en fonction du nombre de Grashof sont présentées pour les données mesurées de transport de chaleur avec quatre rapports de diamètres différents, la meillure corrélation s'accordant avec l'expérience à moins de 15,5 pour cent près. Le nombre de Grashof basé sur la distance entre les sphères variait de 2×10^4 à $2{,}6 \times 10^6$.

Zusammenfassung—Eine experimentelle Untersuchung der freien Konvektion von Luft zwischen zwei isothermen, konzentrischen Kugeln verschiedener Durchmesserverhältnisse von 1,19 bis 3,14 wird beschrieben. Die Ergebnisse einer visuellen Studie, die deutlich drei Arten von Strömungsmuster erkennen lässt, sind zusammengefasst. Die gemessenen Temperaturprofile werden unter Zugrundelegung von fünf typischen Formkennzeichen eigehend analysiert. Mit Ausnahme der angenommenen Bizellularströmung zur Erklärung der Profile bei kleinstem Durchmesserverhältnis sind alle Profilerscheinungen auf Grund der beobachteten konvektiven Strömungsmuster gedeutet. Zwei Nusselt–Grashof Korrelationen sind für den gemessen Wärmeübergang bei vier verschiedenen Durchmesserverhältnissen angegeben wobeit für die bessere Korrelation nur eine Streuung von 15,5 Prozent auftritt. Die mit der Spaltweite gebildete Grashofzahl erstreckte sich von $2{,}0 \times 10^4$ bis $3{,}6 \times 10^6$.

Аннотация—Описывается экспериментальное исследование естественной конвекции воздуха, заключенного между двумя изотермическими концентрическими сферами с отношением диаметров от 1,19 до 3,14. Дается обобщение результатов визуального исследования, определившего существование трех различных режимов течения. Подробно анализируются результаты измерений температурных профилей на основе пяти

типичных параметров форм профилей. За исключением случая, когда для объяснения профилей, полученных для наименьших отношений диаметров, принимается поток с двумя зонами циркуляции, все свойства профилей объясняются, исходя из наблюдаемых режимов течения. Для четырех различных отношений диаметров приводятся два соотношения Нуссельта–Грасгофа, описывающие полученные данные по теплообмену, причем наиболее удачное соотношение описывает данные с точностью до 15,5%. Число Грасгофа, основанное на толщине зазора, составляло от $2{,}0 \times 10^4$ до $3{,}6 \times 10^6$.